Journal of Statistical Physics, Vol. 92, Nos. 5/6, 1998

Metastability and Spinodal Points for a Random Walker on a Triangle

Peter F. Arndt[1] **and Thomas Heinzel**[1]

Received January 27, 1997; final June 3, 1998

We investigate time-dependent properties of a single-particle model in which a random walker moves on a triangle and is subjected to nonfocal boundary conditions. This model exhibits spontaneous breaking of a $\mathbf{Z}_2$ symmetry. The reduced size of the configuration space (compared to related many-particle models that also show spontaneous symmetry breaking) allows us to study the spectrum of the time evolution operator. We break the symmetry explicitly and find a stable phase, and a metastable phase which vanishes at a spinodal point. At this point, the spectrum of the time evolution operator has a gapless and universal band of excitations with a dynamical critical exponent $z = 1$. Surprisingly, the imaginary parts of the eigenvalues $E_j(L)$ are equally spaced, following the rule $\Im E_j(L) \propto j/L$. Away from the spinodal point, we find two time scales in the spectrum. These results are related to scaling functions for the mean path of the random walker and to first passage times. For the spinodal point, we find universal scaling behavior. A simplified version of the model which can be handled analytically is also presented.

KEY WORDS: Random walk; phase transitions; spontaneous symmetry breaking; spinodal points; free energy functional; universal scalings.

1. INTRODUCTION

Spontaneous symmetry breaking in non-equilibrium statistical mechanics was recently observed in several one-dimensional many-particle models.[1–5] In this paper we consider a single particle random walker model[6] which exhibits symmetry breaking of a $\mathbf{Z}_2$ symmetry. We investigate the spectrum of the time evolution operator and stationary and time-dependent properties. The random walker moves in the two-dimensional geometry of a discretized right-angled triangle. In the interior of the triangle it may hop

[1] Physikalisches Institute, 53115 Bonn, Germany.

0022-4715/98/0900-0837$15.00/0

locally to neighbouring sites, whereas on the two short sides it may jump non-locally to a corner. Unusually for a one particle model the simple model, studied here shows spontaneous symmetry breaking. Considering the infinite volume limit, the particle stays in one corner of the triangle and no longer reaches the opposite corner which is reflected under the symmetry. This yields two equally stable phases.

Breaking the symmetry explicitly by an "external field," one of the stable phases first becomes meta-stable, before one reaches a spinodal point where it becomes unstable, if the field is sufficiently strong enough. Hence one can investigate metastability and spinodal points in non-equilibrium processes with the simple random walker model.

The random walker on a triangle (RWT) model is defined as follows. The walker moves on the triangle

$$\mathcal{T}_L = \{(j, k) \mid j, k \text{ integer } s > 0 \text{ with } j + k \leqslant L\}.$$

We define the following processes for the random walker at site (j, k) where p is the probability of a transition in an infinitesimal time step dt:

$$\begin{aligned}
&(j,k) \to (j-1,k) && \text{if} \quad j>1 \quad \text{with} \quad p = a(1+h)\,dt \\
&(j,k) \to (j,k-1) && \text{if} \quad k>1 \quad \text{with} \quad p = a(1-h)\,dt \\
&(j,k) \to (j-1,k+1) && \text{if} \quad j>1 \quad \text{with} \quad p = b(1+h)\,dt \\
&(j,k) \to (j+1,k-1) && \text{if} \quad k>1 \quad \text{with} \quad p = b(1-h)\,dt \\
&(1,k) \to (1,L-1) && \text{with} \quad p = c(1+h)\,dt \\
&(j,1) \to (L-1,1) && \text{with} \quad p = c(1-h)\,dt
\end{aligned} \tag{1.1}$$

The first four processes are local hops to neighbouring sites on the triangle, the last two are non-local jumps to the corners $(1, L-1)$ and $(L-1, 1)$ respectively. For $h = 0$ the definitions are invariant under reflection on the line $j = k$. We fix the unit of time choosing $c = 1/2$. This renders the probability rates dimensionless. The defined dynamics is the same as the one considered in ref. 6 up to a relabelling of the sites.

In the following we also impose the condition $a + b = 1/2$, which makes the RWT model the "zero-temperature" limit of a three-state model[1, 6] which shows spontaneous *CP* symmetry breaking. (Therefore the reflection symmetry of the RWT model will also be denoted as *CP* symmetry in the following.) It would be interesting to study the general case $a + b \neq 1/2$ as well. In the three-state model, positive and negative particles

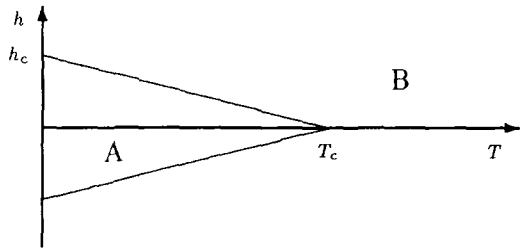

Fig. 1. Simplified phase diagram of the three-state model. In the "low-temperature" regime A the symmetry is spontaneously broken for $h=0$ where h is the strength of a symmetry breaking field. It is separated by a line of spinodal points from the "high-temperature" regime B.

hop among vacancies on a one-dimensional chain. The C operation interchanges positive and negative particles, and the P operation interchanges left and right on the chain. The investigation of the free energy functional, and of the flip times between stable and meta-stable phases, leads to the phase structure given in Fig. 1.[8] In the CP-symmetric case, one finds two broken phases[7] for "low temperatures" (in this model the output rates of the particles play the role of a temperature) and a disordered phase for "temperatures" above T_c. At the critical point ($T=T_c$, $h=0$), one finds a dynamical critical exponent (see Section 2 and ref. 17 for a definition) $z=2$, which is connected with the appearance of shocks.[8-11] Breaking the symmetry explicitly, one finds a "low-temperature" regime A with a stable and a metastable phase. This regime is separated by a spinodal line from the regime B (Fig. 1). At the spinodal line, a previous investigation suggested $z=1$ for $h\neq 0$.[8] This motivated us to study time-dependent properties, metastability and spinodal points in more detail. All these are manifestly associated with non-equilibrium models.[12]

Another model which shows spontaneous CP symmetry breaking is the two-state (particles and vacancies, the C operation interchanges these) asymmetric exclusion model.[2-4] The symmetry is broken on the coexistence-line. There the free energy functional is flat (see Appendix A in ref. 8) like in the model discussed above[1,8] at the phase transition point and like in equilibrium physics. In the spontaneously broken stationary state, shock profiles (connected with a dynamical critical exponent $z=2$) appear. But breaking the symmetry one does not find a region with a metastable phase, and hence there are no spinodal points present in the model.

The time evolution of the RWT model is given by the master equation[13]

$$\frac{d}{dt}|p\rangle = -H|p\rangle \tag{1.2}$$

where $|p\rangle$ is the vector of the probabilities $P(j, k)$ of finding the random walker at site (j, k). The "hamiltonian" H is the time evolution operator and is determined by the processes (1.1). The stationary properties of the system are given by the ground state $|p_0\rangle$ with $H|p_0\rangle = 0$, and the dynamical properties are given by the excitations of H.

The configuration space of many-particle models grows exponentially with the system size in contrast to the configuration space of the RWT model which has dimension $L(L-1)/2$. This polynomial dependence on L enabled us to investigate the spectrum of the model. By numerical diagonalization of the hamiltonian, we found an interesting two band structure of the spectrum, which leads to two gaps or time-scales. At the spinodal point $h_c = a/(1-a)$ (cf. ref. 6), one scale vanishes with critical exponent $x = 2$ and the lower part of the spectrum has the form $E_j = ak_j/L$. The constants k_j are universal, and do not depend on the remaining parameter a. This reminds one of the critical spectrum of a quantum spin chain related to a nonformal field theory. As a surprise, the imaginary parts of the constants k_j have the form $\mathcal{I}k_j = j\mathcal{I}k_1$. For the real parts, we do not find any regularity.

The value of h_c has already been conjectured in ref. 6. It is also predicted by taking the "zero-temperature" limit of the mean-field results for the three-state model discussed in ref. 8. There, mean-field theory was found to be compatible with simulations for small "temperatures" (output rates).

Besides the study of the time evolution operator one can, as with other models, investigate the free energy functional (FEF) of the RWT model. This functional f is defined as:[8, 14]

$$f_L(d) = -\frac{1}{L}\log P_0(d, L), \qquad f(d) = \lim_{L\to\infty} f_L(d) \tag{1.3}$$

where d is an order parameter of the model and $P_0(d, L)$ denotes the corresponding stationary probability distribution.[8] For the RWT model, we take

$$d = (j-k)/L \tag{1.4}$$

as the order parameter.

Analogously to the "low-temperature" regime of the three-state model, one finds that the FEF of the RWT model has two global minima $(d = -1, +1)$ in the CP-symmetric case $(h = 0)$. In the limit $L \to \infty$, the symmetry is spontaneously broken and there are two equally stable phases with $d = \pm 1$. For $O < h < h_c$, the dynamics (1.1) favors the movement to lower values of the order parameter and the FEF has a global minimum

($d=-1$) and a local minimum ($d=+1$). This leads to the existence of a stable and a meta-stable phase in the infinite volume limit ($L\to\infty$), the random walker staying near the favored corner $F=(1, L-1)$ and the unfavored corner $U=(L-1, 1)$ respectively. Above h_c there exists only one phase, the random walker always staying around F. This is also reflected in the spectrum of the hamiltonian (1.2), since one has two ground states for $L\to\infty$ and $h<h_c$ and only one for $h>h_c$.

It is also possible to measure the flip time from one phase to the other using Monte Carlo simulations. At the spinodal point, one observes a discontinuity in the passage time from the corner U to the corner F. At and above h_c, the average time taken to reach the corner F grows linearly with L. However, there is a discontinuity in the proportionality constant as one approaches h_c from above. The linearity above h_c can be explained by a mean-field argument, the linearity at h_c cannot. The time taken to reach the corner U and the time taken to reach the corner F for $h<h_c$ grow exponentially with L.

Using Monte Carlo simulations, one can also investigate the movement of the random walker starting from specific initial conditions. Analysing the mean path, one again identifies two time scales away from the spinadal point, and at the spinodal point, one again finds universal behavior.

All the results found here for the RWT model are in accordance with the results found for the three-state and the asymmetric diffusion models. But the detailed analysis of the spectrum of the time evolution operator now suggests a link between the time-scales found in the spectrum, the time-scales found in the flip times, and the scales one observes in the movement of the random walker. This was not observed before.

The random walker on a triangle can be simplified to a random walker on a right angle (RWRA) model which can be handled analytically while still possessing a meta-stable phase. This is done taking $b=0$ and keeping only the points $(j, k)\in\mathcal{T}_L$ with $j=1$ or $k=1$. That is, we consider only the movement along the j- and k-axes, where macroscopic jumps occur. In an infinitesimal time interval dt the following processes can occur with a probability p:

$$\begin{aligned}
&(j,1)\to(j-1,1) && \text{if } j>1 \text{ with } p=a(1+h)\,dt\\
&(j,1)\to(L-1,1) && \text{with } p=c(1-h)\,dt\\
&(1,k)\to(1,k-1) && \text{if } k>1 \text{ with } p=a(1-h)\,dt\\
&(1,k)\to(1,L-1) && \text{with } p=c(1+h)\,dt
\end{aligned} \tag{1.5}$$

The RWRA model is essentially a one-dimensional (albeit non-local) random walker model. Again we limit our investigation to the case $c=1/2$

(this fixes the unit of time) and $a \equiv a + b = 1/2$. We checked that takings different from 1/2 does not change the physics of the RWRA model. One is able to calculate exactly a characteristic equation for the eigenvalues of the time evolution operator, the free energy functional and the flip times. The spinodal point is at $h_c = 1$. Since all rates in (1.5) have to be positive one can study with the RWRA model only the regime below the spinodal point. The results are given in Appendix C.

The paper is organized as follows. In the next section, we present our results on the spectrum of the hamiltonian of the RWT model. We identify two time scales, one of which vanishes at the spinodal point. At this point, the low-lying excitations acquire a universal L^{-1} dependence yielding $z = 1$. We also show that finite-size scaling relations hold.

In Section 3, we compute the FEF of the RWT model and present our Monte Carlo results on the passage times from the favored corner F to the unfavored corner U and vice versa. Two scales can be measured and related to the depths of the minima of the FEF and to gaps in the spectrum of H found in Section 2.

In Section 4, we give results on the movement of the random walker that mirror the scales found for the spectrum (Section 2). At the spinodal point, one finds a non-trivial universal behavior that also reflects the dynamical exponent $z = 1$. Section 5 contains our conclusions.

In Appendix A, we give some simple results for the movement of the random walker for h above the spinodal point. In Appendix B we explain the connection between the flip times and the spectra of models with absorbing configurations. In Appendix C we investigate the random walker on a right angle model.

2. SPECRTRUM OF THE HAMILTONIAN

Using a modified version of the Arnoldi algorithm,[15] we have calculated the low-lying eigenvalues (up to the 30th level) of the time evolution operator H for $L \leqslant 220$, various values of h, and $a = 0.001$, 0.1, 0.25, 0.4. Apart from the ground state "energy" $E_0(L) \equiv 0$, the further eigenvalues of the non-hermitian matrix H are positive, or complex with positive real parts. Since the hamiltonian matrix has real entries only, complex eigenvalues come in conjugated pairs. Typical results for the real part of the spectrum (for $a = 0.25$, $h = 0.3$) are shown in Fig. 2. One identifies two bands of excitations leading to the gaps (time scales) m_1 and m_2 in the large L limit. Note that the excitations correspond to energy gaps, since the ground state energy of H is zero for any system size.

Values for the large L limit were extrapolated from data for finite L using the Bulirsch-Stoer algorithm.[16]

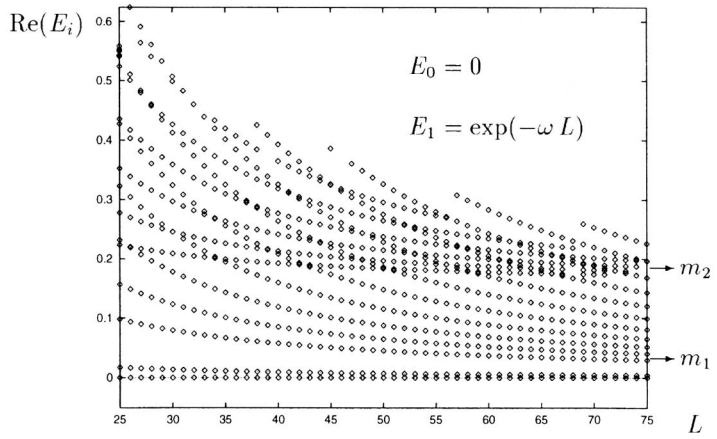

Fig. 2. Dependence of the spectrum on system size. The data is from numerical diagonalization for $a = 1/4$, $h = 0.3$. Shown are the real parts of the eigenvalues of H. The gaps m_1 and m_2 extrapolate to finite values as seen in Fig. 3.

The most important observation is that there exists a critical spinodal point at $h_c = a/(1-a)$ (see Fig. 3). At this point, the system loses one of its time scales ($m_1 = 0$) and acquires a band of excitations with a universal L^{-1} dependence.

The results for the spectrum of H can be summarized as follows:

• *first excitation*: For $h < h_c$ the first excited energy level approaches zero as

$$E_1 \propto \exp(-\omega L) \tag{2.1}$$

This excitation is real, the higher excitations are complex conjugated pairs. Thus, in the limit $L \to \infty$, there are two ground states. Linear combinations of the eigenvectors give two phases.[7] For $h = 0$ they are equally stable, while for $h > 0$ one of them is stable, and the other is meta-stable. The two phases correspond to minima of the free energy functional at $d = 1$ and $d = -1$ (see Section 3). The meta-stable phase vanishes at the spinodal point h_c. Above h_c, there is only one ground state for $L \to \infty$, i.e., none of the excited levels approaches zero.

• *higher excitations*: Above E_0 and E_1, there are two bands of complex eigenvalues of the form

$$E_j^{(1)}(L) = m_1 + k_j^{(1)}/L + \cdots \tag{2.2}$$

$$E_j^{(2)}(L) = m_2 + k_j^{(2)}/L + \cdots \tag{2.3}$$

The gaps m_1 and m_2 are real, whereas the constants $k_j^{(i)}$ have imaginary parts, such that one has complex conjugated pairs of eigenvalues. One finds that m_1 is proportional to ω. For $a=0.25$, we find $m_1=0.57(4)\,\omega$.

For $h=0$ one has $m_1=m_2$ and the constants $k_j^{(1)}=k_j^{(2)}=k$ are independent of j, i.e., the $1/L$ term is the same for all excitations in contrast to Eqs. (2.2) and (2.3) for $h>0$. There are two ground states (compare Eq. (2.1)), corresponding to equally stable phases.

For $h>h_c$ the excitations again come in the form of two bands as in Eqs. (2.2) and (2.3).

- *lower gap*: For $h\to h_c$, the lower gap m_1 vanishes, as does ω, which is proportional to m_1. For $h<h_c$, the gap is given by $m_1=\lim_{L\to\infty} E_2(L)$. Above h_c, the first excitation does not give a second ground state for $L\to\infty$ and one finds a non-zero gap $m_1=\lim_{L\to\infty} E_1(L)$. The gap m_1 given by

$$\begin{aligned} m_1 &= 0.42(2)(h_c-h)^x \qquad \text{for} \quad h<h_c \\ m_1 &= 0.46(2)(h-h_c)^x \qquad \text{for} \quad h>h_c \end{aligned} \tag{2.4}$$

where the numbers are given for $a=0.25$. Note that these equations are valid for any h and not only in the vicinity of h_c. One finds an exponent $x=2.00(1)$ for $h<h_c$ and $h>h_c$. Extrapolated values for the m_i are shown in Fig. 3.

The position of the minimum of the parabola Eq. (2.4) determines the spinodal point at $h_c=a/(1-a)$ with a precision of two digits.

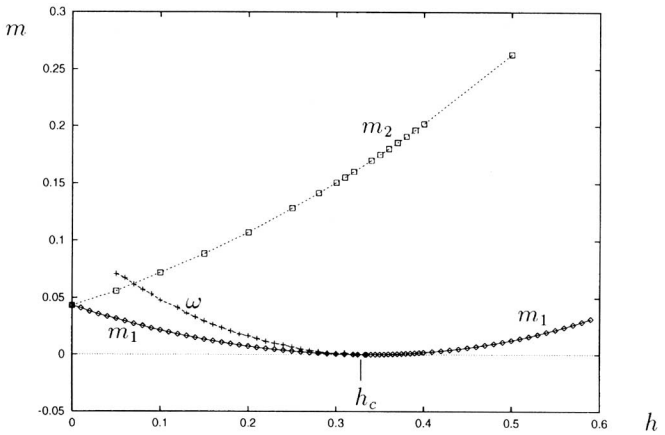

Fig. 3. Length scale ω, and upper and lower gaps m_1 and m_2 for $a=(1/4)$. The values given are extrapolated from data of numerical diagonalization of H up to $L=220$.

• *upper gap*: The scale m_2 increases monotonically with h over the entire range $0 \leqslant h < 1$. One finds

$$m_2 = 0.48(2)\, h^{1.22(2)} + 0.043(2) \tag{2.5}$$

for $a = 0.25$.

• *lower band of excitations at $h = h_c$*: At the spinodal point, the lower band is of the following form:

$$\begin{aligned} E_0 &= 0 \\ E_1 &= a\frac{k_1^{(1)}}{L} + \frac{\text{const.}}{L^{3/2}} + \cdots \quad \text{real} \\ E_j &= a\frac{k_j^{(1)}}{L} + \frac{\text{const.}}{L^{3/2}} + \cdots \quad j \geqslant 2, \text{ complex conjugated pairs} \end{aligned} \tag{2.6}$$

with the extrapolated values $k_j^{(1)}$ given in Table I. One has universality: apart from the normalization constant a ("speed of light"), the leading terms are the same for any critical point $h_c(a) = a/(1-a)$. Extrapolation of the $k_i^{(1)}$ for $a = 0.25, 0.4, 0.1$ gives the same result with 5 digits precision. At the spinodal phase transition, the dynamical critical exponent[17] is $z = 1$ (i.e., the exited levels vanish in leading order with L^{-1}), as was found for the three-state diffusion model where, however, this was only seen fo,r the first excitation.[8]

The imaginary parts of the numbers $k_j^{(1)}$ follow (see Table I)

$$\mathcal{I}(k_j^{(1)}) = 12.81(1)\, j \tag{2.7}$$

This equidistant spacing comes as a surprise and we do not know its reason. For quantum spin chains related to a conformal field theory one

Table I. Excited Levels of H at h_c: $E_j = a(k_j/l)$[a]

level	$\mathcal{R}(k_j^{(1)})$	$\mathcal{I}(k_j^{(1)})$	$\mathcal{I}(k_j^{(1)})/12.81$
1	1.7080	0	0
2	8.4980	12.7663	0.997
4	10.368	25.771	2.012
6	11.504	38.548	3.009
8	12.324	51.241	4.000
10	12.97	63.89	4.988
12	13.5	76.52	5.994

[a] Complex excitations come in conjugated pairs.

expects regularities (nonformal towers) for the real parts of the $k_j^{(1)}$. However, we could not detect any such structure looking at the real part of the spectrum. This should be a result of the reduced state space of the RWT model. Because of the large configuration space of the full three-state model, a similar analysis was not possible there. For the higher band of excitations at the spinodal point, one again has the form of Eq. (2.3).

• *finite-size scaling analysis*: Finite-size scaling relations, which describe the behavior of finite quantum spin chains in the vicinity of an (equilibrium) critical point of the infinite system,[18] apply also to the (non-equilibrium) RWT model at h_c. Consider the curves

$$F_L: h \to LE_1(h, L) \tag{2.8}$$

The critical point h_c can be determined from extrapolation of the crossing points $h_{\text{cross}}(L)$ of the curves F_L and F_{L-1}. Indeed one finds

$$\lim_{L \to \infty} h_{\text{cross}}(L) = 0.3333(2) = h_c \tag{2.9}$$

for $a = 0.25$. This isle the most precise numerical determination of h_c.

Following the finite-size scaling hypothesis, one can also determine the critical exponent x in a way different from that of Eq. (2.4).[18] From the available data up to $L = 220$, one again finds $x = 2.0(2)$.

In the following sections, we discuss further properties of the RWT model that can be related to the scales of the spectrum and to the universality at the critical point. The scale ω can be linked with flip times and the stationary FEF (see next section). In Section 4, we present dynamic quantities related to the properties of H, specifically to the gaps m_i.

3. FREE ENERGY FUNCTIONAL AND FLIP TIMES BETWEEN PHASES

We have investigated the behavior of the stationary probabilities $P_0(j, k)$ for different h. These probabilities were determined from the stationary state as computed by numerical diagonalization of the hamiltonian (see Section 2). First, we remark that for $h = 0$ all eigenstates are also eigenstates of the CP operation. We find that the eigenvectors corresponding to the complex conjugated pairs of eigenvalues $E_j^{(1)}$ of the lower band of excitations (2.2) are CP^+ for j even and CP^- for j odd.

One also finds that, for any h and finite L, the eigenvector $|p_0\rangle$ with eigenvalue $E = 0$ is the only vector that directly corresponds to a probability distribution, i.e. all its entries are positive. In the case $h = 0$, $|p_0\rangle$ has CP^+ symmetry.

Hence, for $h=0$, the free energy functional $f(d)$, defined in Eq. (1.3), is symmetric under the inflection $d \to -d$. (From the data, one finds that the free energy functional is a well defined limit as was already known for the asymmetric exclusion model and the three-state diffusion model.[8]) There are minima at $d=-1$ and $d=1$ and a maximum at $d=0$. The minima correspond to the two equally stable phases (see Fig. 4). This is basically the same situation as for the CP-symmetric three-state model in the "low-temperature" phase.

For $0<h<h_c$, one has a global minimum at $d=-1$ and a further, shallower minimum at $d=1$ (see Fig. 4). This reflects the fact that one of the phases becomes meta-stable. One can define two scales:

$$\begin{aligned} \nu_{\text{large}} &= f_{\max} - f(-1) \\ \nu_{\text{small}} &= f_{\max} - f(1) \end{aligned} \tag{3.1}$$

where $f_{\max}$ is the maximum value of $f(d)$. We shall relate these scales to the time the system needs to flip from one minimum to the other. At h_c, the second minimum of f (and hence the meta-stable phase) vanishes. This cannot be seen in Fig. 4 but can be inferred from the results for smaller lattice sizes. For $h \geqslant h_c$, the free energy has only one minimum at $d=-1$.

Analysis of the eigenvectors of H that become the steady states in the large L limit, and the relation of the RWT to the three-state diffusion model, have given the result that below h_c there are two distinct phases

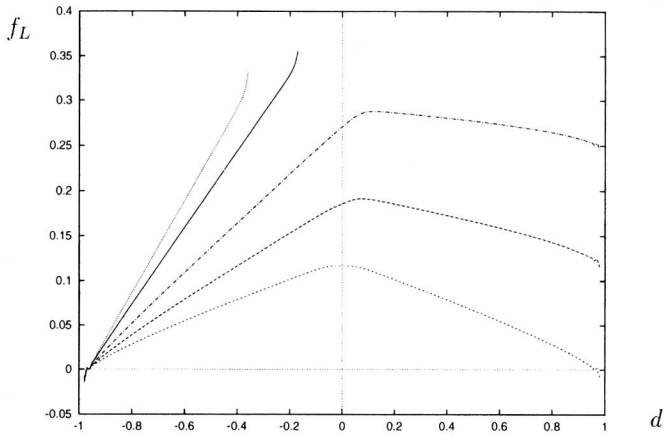

Fig. 4. The free energy functional $f_L(d)$ for $a=1/4$, $L=100$ and $h=0.0, 0.1, 0.2, 0.3333, 0.4$. The values are shifted by the value $f_L(-1)$. The data is generated by numerical diagonalization of the hamiltonian. Since the precision is limited to 10^{-12} the curves for larger h cannot be fully determined.

with order parameter values $d=1$ and $d=-1$. Above h_c, however, there is only one phase: the walker stays near the favored corner F of $\mathcal{T}_L$. This can be verified with Monte Carlo simulations. In a way similar to that for three-state diffusion model,[1,8] one can measure the time for the RWT model to flip from one phase to the other. One finds that, for large L and $h<h_c$, in the neighbourhood of a corner $F=(1, L-1)$ or $U=(L-1, 1)$, the random walker moves through the configurations on a shorter time scale than is needed to get from one corner to the other. This allows one to measure the flip times T_{long} from favored to unfavored and T_{short} from unfavored to favored phase as average first passage times from F to U and U to F respectively.

With $c=1/2$ and $a+b=1/2$, the unit of time is defined such that, on average, the random walker moves one step (1.1) per unit. From the simulations, one finds that, to leading order, the flip times are given by

$$T_{\text{long}} \propto \exp(\mu_{\text{long}} L) \qquad \text{for any } h \tag{3.2}$$

$$T_{\text{short}} \propto \begin{cases} \exp(\mu_{\text{short}} L) & \text{for } h<h_c \\ L & \text{for } h \geqslant h_c \end{cases} \tag{3.3}$$

For $h<h_c$, the time intervals the random walker spends alternately near either corner increase exponentially with L. The fraction of time in the meta-stable region decreases exponentially. In this sense, for $h<h_c$, there are a meta-stable and a stable phase. Results of the measurement for $a=0.25$ and $h=0.1$ are presented in Fig. 5.

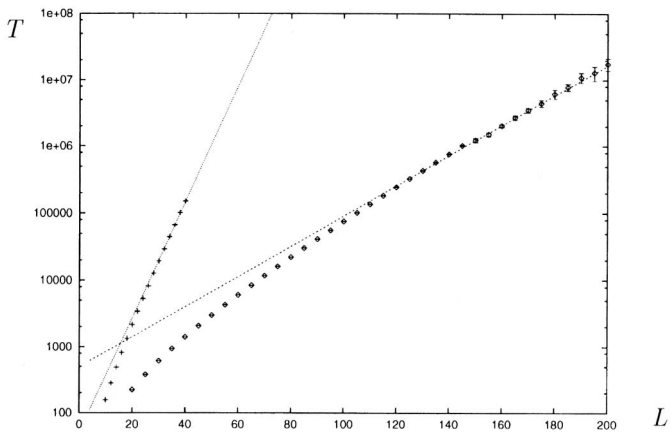

Fig. 5. The flip times $T_{\text{short}}(L)$ and $T_{\text{long}}(L)$ for $a=1/4$ and $h=0.1$. The fitted lines are given by $50\exp(0.2L)$ and $500\exp(0.052L)$.

For $h > h_c$, the proportionality constant in Eq. (3.3) can be calculated by a simple argument, see Appendix A:

$$T_{\text{short}}^{h>h_c} = \frac{L}{h + a(1-h)} = \frac{1+h_c}{h+h_c} L \tag{3.4}$$

In contrast, the appearance of a linearly growing flip time at $h = h_c$ is non-trivial. One finds the form

$$T_{\text{short}}^{h_c} = \frac{L}{a} - \frac{\gamma L^{1/2}}{a} + \text{const.} \tag{3.5}$$

where $\gamma = 0.57(6)$ is a positive constant and independent of a to a precision of about 10%. Up to the normalization a, the short flip time is, to leading order, a universal function of L as are the leading terms of the lower spectrum Eq. (2.6). The appearance of a universal linear flip time is linked to the universal $1/L$ spectrum of the hamiltonian, compare Eq. (2.6). One can ask how general this universal behavior is. Similar investigations for other models remain to be done.

Note that from (3.4) and (3.5) one finds that to leading order

$$\lim_{h \to h_c} T_{\text{short}}^{h>h_c} = 2T_{\text{short}}^{h_c} \tag{3.6}$$

Hence there is a discontinuity in the flip time $T_{\text{short}}^{h_c}$. At the spinodal point, $T_{\text{short}}^{h_c}$ has a special L dependence, essentially different from its behavior above or below this point.

The values of ν_{small} and ν_{large} in (3.1), determined from numerical diagonalization of H for $L \leqslant 140$, and measurement of the flip times, up to $L = 200$ for T_{short} and $L = 40$ for T_{long}, yield the following result:

$$\begin{aligned} \mu_{\text{short}} &= \nu_{\text{small}} \qquad \text{for} \quad h < h_c \\ \mu_{\text{long}} &= \nu_{\text{large}} \qquad \text{for any } h \end{aligned} \tag{3.7}$$

As an example for $h = 0.1$ and $a = 0.25$, we find the values $\mu_{\text{short}} = 0.044(3)$ and $\mu_{\text{long}} = 0.16(2)$ (see Fig. 5) which is to be compared with $\nu_{\text{small}} = 0.05(5)$ and $\nu_{\text{large}} = 0.17(2)$ (see Fig. 4). For $h = 0$ and $a = 0.25$ the equations (3.7) can be checked to three digits; the precision decreases with increasing h to about one digit at $h = 0.3$. (Finite-size corrections to (3.1), (3.2) and (3.3) become more important for higher h due to crossover effects to the linear regime for $h \geqslant h_c$.)

Equation (3.7) is interesting because it relates (steady state) properties of the free energy functional $f(d)$ with (dynamical) flips between phases.

This is unexpected for a non-local model without detailed balance. For the RWRA model (Appendix C) an analogous link can be made analytically. Also, for the three-state diffusion model, similar observations, albeit with less precision, were made in ref. 8.

One also finds that $\mu_{\text{short}} = \omega$ (recall that $E_1 \propto \exp(-\omega L)$ is the first excitation of the hamiltonian, see Eq. (2.1)). For $h = 0.1$ and $a = 0.25$ the value of ω from numerical diagonalization is 0.048(3). The reason for this connection, together with an analogous expression for μ_{long} is given in Appendix B. where we consider modified models with absorbing configurations.

4. TIME SCALES AND CRITICALITY IN THE MOVEMENT OF THE RANDOM WALKER

To find macroscopic physical quantities reflecting the time scales of the spectrum and the critical behavior at h_c, we investigated the movement of the random walker starting from the specific initial positions $U = (L-1, 1)$ (unfavored corner) or $F = (L-1, 1)$ (favored corner). In the following we concentrate on the time dependence of the order parameter coordinate. Defining the average order parameter distance from the starting point as

$$s(t) = \frac{|\langle d(t) - d(0) \rangle|}{2} \tag{4.1}$$

the start configuration corresponds to $s = 0$ and the opposite corner of the triangle $\mathcal{T}_L$ to $s = 1$.

Start at Unfavored Corner

First, we consider the random walker starting at the point U. We shall see that the movement from the unfavored to the favored corner is linked with the lower excitations of the hamiltonian.

Typical pictures of the walker's position $s(t)$ are given in Figs. 6–9. In Fig. 6 we show the product $L \cdot s$ as a scaling function of t, in Fig. 7 the distance s as a scaling function of t/T_{short} (both for h below the critical point), and in Figs. 8 and 9 the distance s as a scaling function of t/L (at and above the critical point respectively). One observes the following properties of the scaling functions:

- $h < h_c$: The random walker stays near U for an average time exponentially increasing with L (Eq. (3.3)). For large L, the path near the unfavored corner (start) is described by the scaling function

$$Ls(t) \propto (1 - \exp(-\lambda t)) \tag{4.2}$$

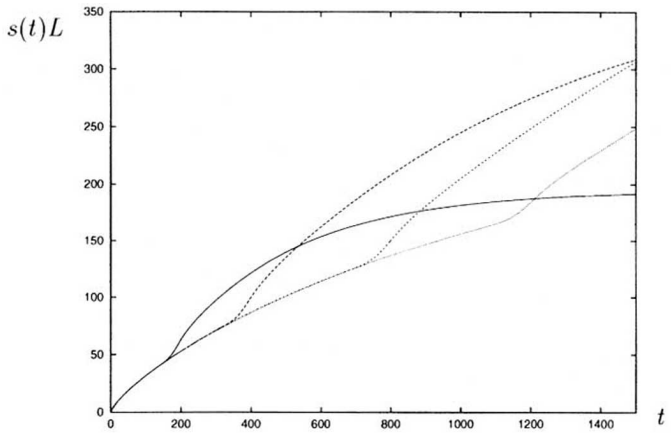

Fig. 6. Average distance $s(t)$ from starting point $U=(L-1, 1)$. Data from simulation of the RWT model for $a=1/4$, $h=0.3$ and system sizes $L=100$ (solid), 200 (long dashed), 400 (short dashed), 600 (pointed). The scaling variable is t.

Here we find $\lambda = 1.8(2) \cdot m_1(h)$ for $a=0.25$. Due to the distribution of flip times for finite L the walker leaves this regime at different times (Fig. 6).

For the approach to the favored corner, one observes a different scaling (Fig. 7). From the data, one finds that s is given by

$$s(t, L) = s_\infty - \exp\left(-\lambda \frac{t}{T_{\text{short}}(L)}\right) \tag{4.3}$$

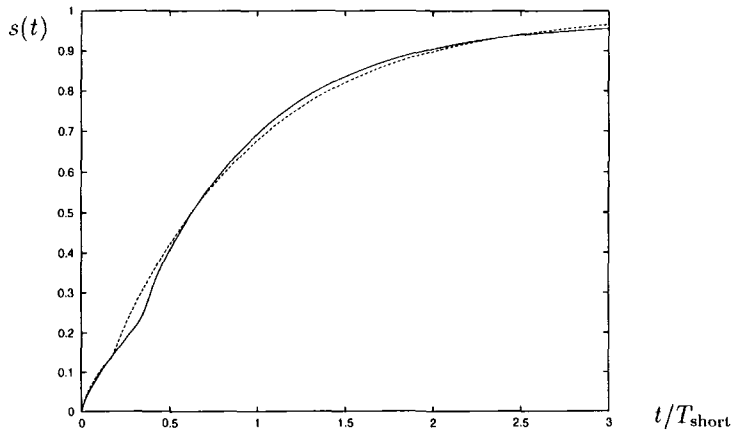

Fig. 7. Average distance $s(t)$ from starting point $U=(L-1, 1)$. Data from simulation of the RWT model for $a=1/4$, $h=0.3<h_c$. The solid curve represents the data for $L=100$, the dashed for $L=600$.

where

$$s_\infty = \lim_{t \to \infty} s(t) = 1 - \frac{\text{const.}}{L} + \cdots \tag{4.4}$$

In Eq. (4.3), the constant $\lambda = 1.15(3)$ is independent of a. The approach to the favored corner scales with t/T_{short}. In the scaling of Fig. 7, the initial path (Eq. (4.2) and Fig. 6) of the random walker cannot be seen because it is reduced to a point.

- $h = h_c$: We consider the scaling regime $t \to \infty$ and $L \to \infty$, taking t/L fixed. For $t < T_{\text{short}}/2 = L/2a$, the distance from the starting point increases in leading order linearly with time. We find

$$s(t, L) = \frac{1}{L}\left(\frac{a}{2} t + \delta \sqrt{t} + \text{const.} + \cdots\right) \tag{4.5}$$

where $\delta = 0.17(2)$ independent of a. For large $t > T_{\text{short}}/2$, the random walker approaches $s = 1$ exponentially, as in the case $h \neq h_c$. The scale, however, is the size of the system

$$s(t, L) = s_\infty - (s_\infty - a) \exp\left(-\kappa\left(a\frac{t}{L} - \frac{1}{2}\right)\right) \tag{4.6}$$

with $\kappa = 1.7(1)$ independent of a. Typical data is shown in Fig. 8.

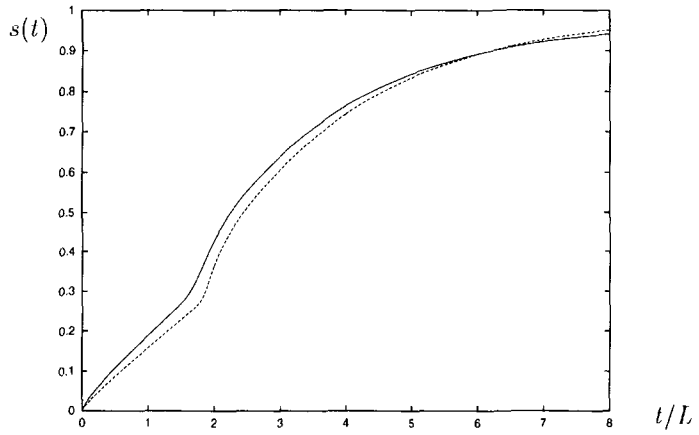

Fig. 8. Average distance $s(t)$ from starting point $U = (L-1, 1)$. Data from simulation of the RWT model for $a = 1/4$, $h = h_c$. The solid curve represents the data for $L = 100$, the dashed for $L = 400$.

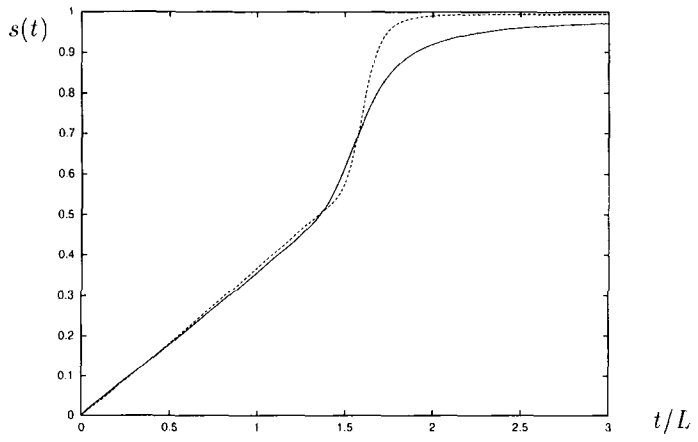

Fig. 9. Average distance $s(t)$ from starting point $U=(L-1, 1)$. Data from simulation of the RWT model for $a=1/4$, $h=1/2>h_c$. The solid curve represents the data for $L=100$, the dashed for $L=400$. The scaling variable is t/L.

At the critical point, the initial path of the random walker Eq. (4.5) is universal and linear to leading order. This reflects again the universal $1/L$ spectrum found for the critical point (2.6). It is remarkable that the exponential scale of Eq. (4.6) is also universal (but not the scaling function). Up to the time normalization (as in Section 2), they do not depend on a and scale with tL^{-1}.

• $h>h_c$: Again we study the scaling t/L fixed taking t and L to infinity. Starting from the unfavored corner U, at first (for $t<T_{\text{short}}$) and to leading order the random walker follows a mean path determined by its velocity vector (see Appendix A). The corrections are exponential in t. We find

$$s(t, L)=ah\frac{t}{L}-\frac{\zeta(1-\exp(\xi t))}{2L} \tag{4.7}$$

With increasing h, the constant ζ decreases and ξ increases and thus the corrections become smaller, consistent with the explanation of Appendix A. For $t>T_{\text{short}}$, one again finds an exponential approach to the final value $s=1$ (see Fig. 9). One has

$$s(t, L)=s_{\infty}-\eta\exp\left(-\left(m_1+\frac{\chi}{L}\right)(t-T_{\text{short}})\right) \tag{4.8}$$

where T_{short} is given by (3.4). The scale is the gap m_1 from the spectrum of the time evolution operator. Following Appendix A, one finds the prefactor

$$\eta = \frac{1}{1 + h/h_c} \tag{4.9}$$

Start at the Favored Corner

We have also studied the path of the random walker starting from F. In that case the critical point h_c does not play a special role. From the simulations, one finds

$$s(t, L) \propto \frac{1 - \exp(\lambda t)}{L} \tag{4.10}$$

where $\lambda = 1.25(5) \cdot m_2(h)$ for $a = 0.25$. This equation is similar to Eq. (4.2), but note that in this case the movement is related to the time scale m_2 that describes a faster movement than the time scale m_1.

In summary, from the study of the movement of the random walker described in this section one can identify different scales. They are related to those excitations of H that describe the movement in question. One finds that the lower band of excitations (slow modes) is related to the path from F to U and the higher band (fast modes) to the movement around the favored corner F. This is confirmed by the results of Appendix B for the model with absorbing configurations. For h_c, we find a scaling function involving only the system size L as a scale, and depending on tL^{-1}. This scaling is analogous to the case of conformal invariance in critical equilibrium systems.

We want to point out that, of course, the described scaling properties can also be found by investigating order parameters different from d.

5. CONCLUSIONS

In this paper, we studied the spectrum of the time evolution operator and other time-dependent properties of the two-dimensional non-local random walker (1.1). This model is a simple example of a class of non-equilibrium models which exhibit spontaneous breaking of a $\mathbf{Z}_2$ symmetry.

The reduced size of the configuration space of the single particle model of this paper allowed us to determine the spectrum numerically with enough precision to extract the gaps (time scales) and the large L limit of the low excitations. For many-particle models a numerical investigation of

the spectrum is much more difficult and has not been done. The investigation of the spectrum of the RWT model led us to the following discoveries.

Breaking the symmetry explicitly with a small $h > 0$, one is left with two phases, a meta-stable and a stable one, in accordance with the fact that the time evolution operator of the model has two ground states in the large L limit. Above the two ground states, one has two bands of excitations corresponding to two time scales.

At the point $h_c = a/(1-a)$ the meta-stable phase becomes unstable and, above that point, one is left with only one ground state and correspondingly one (stable) phase. This spinodal point has very interesting properties. Fixing $h = h_c$, not only does one of the time scales vanish, but the corresponding excitations also acquire the form $E_i = ak_i/L$. Hence, it is universal in the sense that the constants k_i do not depend on the remaining free parameter of the model.

At $h = h_c$, the dynamical critical exponent is $z = 1$, and the time scale vanishes with an exponent $x = 2$. Looking for "conformal towers," we did not find any regularities in the real part of the spectrum, but could show that the imaginary parts of the k_i have equidistant separations. We believe that the $1/L$ dependence on the system size is a more general phenomenon ($z = 1$ for the first excitation had already been found for the three states model in ref. 8) and expect more structure to be found for the spectrum of many-particle-models at their spinodal points. The missing "conformal towers" for the RWT model may be a result of the reduced configuration space. Whether such a spectrum has further deep implications, as would be the case for equilibrium problems where one has conformal invariance, remains uncertain.

Besides the numerical diagonalization, we performed simulations of the model to identify the physical relevance of the time scales. The lower gap is linked with the movement from unfavored to favored phase (slow modes), the higher gap with the movement within the favored phase (fast modes). We could identify different scaling regimes for the movement of the random walker starting at specific sites. The scaling functions reflect the time scales found for the hamiltonian. At the spinodal point, the appropriate scaling variable for the movement starting from the unfavored phase is t/L and the corresponding scaling function is universal.

We also measured the first passage time for the random walker between stable and meta-stable phase. We found that, below the critical point, both these flip times increase exponentially with L. The flip times can be computed from the excitations of a modified model with absorbing configurations (Appendix B). At the critical point, the first passage time from the unfavored to the favored corner of the triangle has a non-trivial, universal linear dependence on L, consistent with the dynamical critical

exponent $z = 1$. The proportionality constant is different, by a factor of two, from its value above the spinodal point where the flip time also increases linearly with L. (There it can be calculated by a simple argument.)

As with the three-state model, we have also investigated the free energy functional as a function of the order parameter d (1.4). Surprisingly for a non-local model without detailed balance (but analogous to the three-state model), we observed a link between steady state properties (the free energy functional) and non-stationary dynamics (flip times).

Those of the described results that relate to the region $h < h_c$ can also be found in a simplified, one-dimensional random walker model (RWRA model, see Appendix C). For this model one can calculate the free energy functional, first excitations and flip times analytically. The further reduction of the configuration space leads to the different critical exponent $x = 1$ instead of $x = 2$.

APPENDIX A. MOVEMENT OF THE RANDOM WALKER FOR $h > h_c$

In the interior of the triangle $\mathscr{T}_L$, the random walker defined by (1.1) has an average velocity of

$$v = \begin{pmatrix} -h - a(1+h) \\ h - a(1-h) \end{pmatrix} \tag{A.1}$$

independent of the site (j, k). here, the first coordinate is along the j-axis (number of $-$ particles) and the second along the k-axis ($+$ particles). The projection onto the direction of the order parameter d is given by

$$v_d = -2h(1-a) \tag{A.2}$$

Repeating the argument of Ref. [6], one sees that for small h both components of v are negative. The walker near either of the corners $(L-1, 1)$ or $(1, L-1)$ drifts towards the j- or k-axis and subsequently jumps back to the respective corner. At $h_c = a/(1-a)$, the velocity is antiparallel to the j-axis. for $h > h_c$, the second component of v is positive, rendering the unfavored corner around $(L-1, 1)$ unstable, because the random walker moves away from the j-axis and the non-local jumps along this axis become irrelevant in leading order. We have checked this with Monte Carlo simulations, (see also Section 4).

Neglecting these non-local jumps, from the mean path given by v one can easily calculate the time taken for a walker starting at $U = (L-1, 1)$ to hit the k-axis and to reach the favored corner. One finds the flip time (3.4). in the same way, (A.2) explains the leading term of (4.7) and (4.9).

APPENDIX B. THE RWT MODEL WITH ABSORBING CONFIGURATIONS

In this appendix, we investigate further the relation of flip times and spectra. We focus on the case where the time that the walker remains in a phase increases exponentially with the system size.

The flip times T_{long} (3.2) and T_{short} (3.3) are defined as first passage times. It is known that the corresponding time scales are related to dynamical properties, i.e. excitations, of a modified model with an absorbing state.[19] An absorbing state is a configuration the system cannot escape from. Here we have to choose U (for T_{long}) or F (for T_{short}) as the absorbing configuration.

We shall first present the general argument (see ref. 19). Consider a reaction diffusion system with an absorbing configuration $\{\beta_{\text{abs}}\}$ and described by a master equation (1.2) with a hamiltonian H_{abs}. The system may start in a configuration $\{\beta_0\}$ at time $t=0$:

$$|p((t=0)\rangle_{\{\beta\}} = \begin{cases} 1 & \text{for} \quad \{\beta\} = \{\beta_0\} \\ 0 & \text{for} \quad \{\beta\} \neq \{\beta_0\} \end{cases} \tag{B.1}$$

where the subscript of a vector denotes the component $\{\beta\}$. Let E_λ and $|p_\lambda\rangle$ be eigenvalues and eigenvectors of the hamiltonian ($E_0 = 0$ being the ground state energy). Note that the ground state $|p_0\rangle$ is given by

$$|p_0\rangle_{\{\beta\}} = \begin{cases} 1 & \text{for} \quad \{\beta\} = \{\beta_{\text{abs}}\} \\ 0 & \text{for} \quad \{\beta\} \neq \{\beta_{\text{abs}}\} \end{cases} \tag{B.2}$$

If H_{abs} is diagonalizable, there exist $a_\lambda \in \mathbf{C}$ such that

$$|p(t=0)\rangle = \sum_\lambda a_\lambda |p_\lambda\rangle \tag{B.3}$$

Obviously, the probability P_{in} that the system has not reached its absorbing state is given by

$$\begin{aligned} P_{\text{in}}(t) &= 1 - P(\{\beta_{\text{abs}}\}; t) \\ &= 1 - (\exp(-H_{\text{abs}} t)\, |p(t=0)\rangle)_{\{\beta_{\text{abs}}\}} \\ &= 1 - \sum_\lambda a_\lambda \exp(-E_\lambda t)\, |p_\lambda\rangle_{\{\beta_{\text{abs}}\}} \end{aligned} \tag{B.4}$$

Denote as $p(t)\, dt$ the probability that the system reaches $\{\beta_{\text{abs}}\}$ during the time interval $[t, t+dt]$. Then

$$p(t)\, dt = P_{\text{in}}(t) - P_{\text{in}}(t+dt) \tag{B.5}$$

Thus, $p(t)$ is given by

$$p(t) = -\frac{dP_{\text{in}}(t)}{dt} = -\sum_{\lambda} a_\lambda E_\lambda \exp(-E_\lambda t)\, |p_\lambda\rangle_{\{\beta_{\text{abs}}\}} \tag{B.6}$$

and its mean value, the flip time, is

$$T = -\sum_{\lambda \neq 0} \frac{a_\lambda\, |p_\lambda\rangle_{\{\beta_{\text{abs}}\}}}{E_\lambda} \tag{B.7}$$

From the last equation, it follows, under the conditions

$$E_1 \propto \exp(-mL), \qquad \lim_{L\to\infty} E_i > 0 \quad \text{for } i \neq 0, 1, \qquad \exists y > 0: \lim_{L\to\infty} L^y a_1 \neq 0$$

that to leading order

$$T(L) \propto \exp(mL) \tag{B.8}$$

The result is similar for any finite number of excited states $E_i \propto \exp(-m_i L)$. In that case, the scale of the flip time is given by the largest m_i, with $\lim_{L\to\infty} L^y a_i \neq 0$ for some y.

On the other hand, if none of the excited levels approaches zero for $L \to \infty$, one has

$$T(L) \leqslant \mathcal{O}(\dim(L)) \tag{B.9}$$

independent of $\{\beta_0\}$ ($\dim(L)$ is the dimension of the configuration space for system size L). This implies that there is only one phase in the large L limit.

We now turn to specific results for the RWT model. We have diagonalized the modified hamiltonian numerically. From the spectra we find the length scales μ_{long} and μ_{short} of the flip times:

- With the favored corner F made absorbing, the scale ω (2.1) remains unchanged as does the gap of the lower band of excitations m_1. This explains the relation $\mu_{\text{short}} = \omega$ (3.7) which is a special case of (B.8). Similar relations are found analytically for the simplified model discussed in Appendix C.

The lower gap vanishes at the critical point h_c and the $1/L$ dependence of the levels is the same as for the non-absorbing RWT model (table C1). The upper gap changes to a new value $m_3 > m_2$.

These results confirm the interpretation that the second ground state (which exists for $h < h_c$, $L \to \infty$) and the lower band of excitations are

linked with the metastable phase and with the movement from the unfavored to the favored corner. The corresponding scales of the spectrum remain unchanged, while the movement within the favored phase, and correspondingly the upper band of excitations, is altered by the absorbing configuration F.

• In the case of an absorbing configuration U in the (originally) unfavored phase, there is more change to the spectrum. There is a first excited state $E_1 \propto \exp(-\omega' L)$ with $\omega' \neq \omega$ for any h, connected with two steady states for $L \to \infty$. This reflects the fact that, with absorption in the corner U, both corners U and F constitute a phase for any h. From (B.8) one has

$$\mu_{\text{long}} = \omega' \qquad \text{for any } h \tag{B.10}$$

analogous to (3.7). This relation is consistent with the numerical data to a precision of about 15%.

Further, the scale ω' is related to m_2 of the RWT model without an absorbing configuration. For $a = 0.25$ one has

$$\omega' = 2.5(2)\, m_2 \tag{B.11}$$

As a further change to the spectrum, the lower band of excitations is shifted to a new band of excitations with, a gap $m_3 > m_2$, while the gap m_2 remains unchanged. The new upper band of excitations is related to movement within the former unfavored corner. Note that $m_3(h)$ takes the same values with either the favored or the unfavored corner made absorbing. The corresponding eigenstates describe the (rapid) movement near an absorbing corner.

APPENDIX C. ANALYTICAL RESULTS FORM THE RWA MODEL

In this appendix, we investigate the model defined by Eq. (1.5). It is expected to give the physics of the RWT model below the spanodal point h_c. We shall indeed see that for the RWRA model there are first passage times from one corner to the other which increase exponentially with L as for the RWT model. We calculate their exact expressions (Eqs. (C.8) and (C.9)) and find the two scales with which these flip times diverge.

We are also able to compute the first excitation (Eq. (C.16)), which becomes a second ground state in the large L limit, and the first excitation for the RWRA model with either of the corners made absorbing (Eqs. (C.20) and (C.21)). The first excitations are proportional to $\exp(-\omega L)$. In

the case of no absorption or absorption at the favored corner, ω is equal to the scale of the short flip time (C.9); and, in the case of the unfavored corner made absorbing, ω is equal to the scale of the long flip time (C.9). All these results are analogous to those for the RWT model, but here they are obtained analytically.

We have also computed the free energy functional Eq. (C.26), whose graph is very similar to that for the RWT model's. As in the RWT model, the height differences $f_{\max} - f_{\min}$ give the scales with which the flip times (C.8)–(C.9) diverge.

C.1. Flip Times

As for the RWT model, for $h = 0$ the random walker stays most of the time near the points $F = (1, L-1)$ and $U = (L-1, 1)$. For $h > 0$, the point F is favored and the stable phase is concentrated around this site.

To calculate the flip time from the meta-stable to the stable phase, we define $D_{j,k}$ as the first passage time from (j, k) to $(1, L-1)$.

Concentrating on the first step of the random walker (in an infinitesimal time interval dt), we find

$$D_{1,k} = (1 - dt)(D_{1,k} + dt) \frac{1-h}{2} dt(D_{1,k-1} + dt) + \frac{1+h}{2} dt(D_{1,L-1} + dt)$$

for $j = 1$, $k = 2, \ldots, L-2$ (cf. ref. 6). This yields

$$D_{1,k} = 1 + \frac{1-h}{2} D_{1,k-1} + \frac{1+h}{2} D_{1,L-1} \tag{C.1}$$

Similarly, the other conditions for the $D_{j,k}$ read

$$D_{j,1} = 1 + \frac{1+h}{2} D_{j-1,1} + \frac{1-h}{2} D_{L-1,1} \qquad j = 2, \ldots, L-2 \tag{C.2}$$

$$D_{1,1} = 1 + \frac{1+h}{2} D_{1,L-1} + \frac{1-h}{2} D_{L-1,1} \tag{C.3}$$

$$\frac{1-h}{2} D_{1,L-1} = 1 + \frac{1-h}{2} D_{1,L-2} \tag{C.4}$$

$$\frac{1+h}{2} D_{L-1,1} = 1 + \frac{1+h}{2} D_{L-2,1} \tag{C.5}$$

From the definition of $D_{j,k}$, the boundary conditions are given by

$$\begin{aligned} D_{1,L-1} &= 0 \\ D_{L-1,1} &= T_{\text{short}} \end{aligned} \tag{C.6}$$

The recurrence relation (C.2) can be solved as

$$D_{j,1} = D_{1,1} \frac{2}{1-h} \left(\left(\frac{1+h}{2} \right)^{j-2} - \left(\frac{1+h}{2} \right)^{j} + 1 \right) \tag{C.7}$$

and the condition (C.5) gives us the flip time

$$T_{\text{short}} = \left(\frac{2}{1-h} \right)^2 \left(\frac{2}{1+h} \right)^{L-2} - \frac{2}{1-h} \tag{C.8}$$

Replacing h by $-h$, we obtain the flip time from favored to unfavored phase

$$T_{\text{long}} = \left(\frac{2}{1+h} \right)^2 \left(\frac{2}{1-h} \right)^{L-2} - \frac{2}{1+h} \tag{C.9}$$

One sees that the flip times diverge exponentially with L. The scales are $\mu_{\text{short}} = \log(2/(1-h))$ and $\mu_{\text{long}} = \log(2/(1+h))$. This implies that there are two ground states in the large L limit. Linear combinations of these give the phases; a stable phase concentrated around $\mathrm{F} = (1, L-1)$, and a metastable around $\mathrm{U} = (L-1, 1)$.

C.2. L Dependence of the First Excitation

With the notation $x_s = P(s, 1)$, $y_s = P(1, s)$ and $x_1 = y_1 = P(1, 1)$, the master equation of the RWRA model reads

$$\frac{\mathrm{d}}{\mathrm{d}t} x_s = -x_s + \frac{1+h}{2} x_{s+1} \qquad s = 2, \ldots, L-2 \tag{C.10}$$

$$\frac{\mathrm{d}}{\mathrm{d}t} y_s = -y_s + \frac{1-h}{2} y_{s+1} \qquad s = 2, \ldots, L-2 \tag{C.11}$$

$$\frac{\mathrm{d}}{\mathrm{d}t} x_1 = -x_1 + \frac{1+h}{2} x_2 + \frac{1-h}{2} y_2 \tag{C.12}$$

$$\frac{\mathrm{d}}{\mathrm{d}t} x_{L-1} = -x_{L-1} + \frac{1-h}{2} \sum_{i=1}^{L-1} x_i \tag{C.13}$$

$$\frac{\mathrm{d}}{\mathrm{d}t} y_{L-1} = -y_{L-1} + \frac{1+h}{2} \sum_{i=1}^{L-1} y_i \tag{C.14}$$

Setting $x_s = \exp(-Et)\, X_s$ and $y_s = \exp(-Et)\, Y_s$, and solving the resulting recurrence relations, we find the condition on an eigenvalue E,

$$0 = E\Bigg(E(1-E)^{2L-3} + \frac{(1-h^2)^{L-1}}{4^{L-1}} - (1-E)^{L-2}(1-h^2)\frac{(1+h)^{L-2}+(1-h)^{L-2}}{2^L}\Bigg) \times \Bigg((1-E)^{2L-5}\left(\frac{1+h}{2}-E\right)\left(\frac{1-h}{2}-E\right)\Bigg)^{-1} \tag{C.15}$$

There is one solution with $E_0 = 0$. The corresponding eigenvector is the steady state for finite L. For $L \ll 1$, the first excited level behaves as

$$E_1 \cong \frac{1}{4}(1-h^2)\left(\frac{1+h}{2}\right)^{L-2} \propto \exp(\omega L) \tag{C.16}$$

Thus, for $L \to \infty$, one has two stationary states resulting in two phases.

The higher spectrum has a two band structure similar to that for the RWT model. The corresponding gaps are $m_1 = (1-h)/2$ and $m_2 = (1+h)/2$. Thus, one finds $\omega = m_1$ for $h \to 1$. (For the RWT model one has proportionality of ω and m_1 for any h, see (2.4).) we point out that for the RWRA model the gap vanishes with a critical exponent $x = 1$, while for the RWT model one finds $x = 2$ (see Eq. (2.4)). This is due to the reduction of the configuration space.

One can compute the large L behavior of the flip times from the L-dependence of the first excited level of a modified model (Appendix B). For the flip time T_{short}, one implements an absorbing site at the stable corner $(1, L-1)$, replacing equations (C.11) and (C.14) by

$$\frac{\mathrm{d}}{\mathrm{d}t} y_s = -y_s + \frac{1-h}{2} y_{s-1} \qquad s = 2,\ldots, L-3 \tag{C.17}$$

$$\frac{\mathrm{d}}{\mathrm{d}t} y_{L-2} = -y_{L-2} \tag{C.18}$$

$$\frac{\mathrm{d}}{\mathrm{d}t} y_{L-1} = \frac{1+h}{2} \sum_{i+1}^{L-2} y_i \tag{C.19}$$

With this, one finds a first excited level

$$E_1^{(1,L-1)\,\text{abs.}} \cong \frac{1}{4}(1-h^2)\left(\frac{1+h}{2}\right)^{L-2} \tag{C.20}$$

With $(L-1, 1)$ absorbing, instead of $(1, L-1)$, one analogously obtains

$$E_1^{(L-1,1)\,\text{abs.}} \cong \frac{1}{4}(1-h^2)\left(\frac{1-h}{2}\right)^{L-2} \tag{C.21}$$

This way, with equations (C.8), (C.9) and (B.8), we find

$$T_{\text{short}} \propto \left(\frac{2}{1+h}\right)^{L-2}$$

$$T_{\text{long}} \propto \left(\frac{2}{1-h}\right)^{L-2}$$

which is indeed consistent with the flip times (C.8) and (C.9) computed directly above.

C.3. The Stationary Probability Distribution

To calculate the probability distribution of the steady state, one has to solve equations (C.10)–(C.14) for $(\mathrm{d}/\mathrm{d}t)\, x_s = (\mathrm{d}/\mathrm{d}t)\, y_s = 0$. One finds

$$X_s = \frac{1}{4} N(1-h^2)\left(\frac{2}{1+h}\right)^s \tag{C.22}$$

$$Y_s = \frac{1}{4} N(1-h^2)\left(\frac{2}{1-h}\right)^s \qquad s = 2,\ldots, L-1 \tag{C.23}$$

$$X_1 = Y_1 = N \tag{C.24}$$

where the normalization N is

$$N = \frac{(1-h^2)^{L-2}}{(2(1-h))^{L-2} + (2(1+h))^{L-2} - (1-h^2)^{L-2}} \tag{C.25}$$

The free energy, defined by (1.3), takes the form

$$f(d) = \begin{cases} \log\left(\dfrac{2}{1-h}\right) - d\log\left(\dfrac{2}{1+h}\right) & \text{for} \quad d \geqslant 0 \\ \log\left(\dfrac{2}{1-h}\right) + d\log\left(\dfrac{2}{1-h}\right) & \text{for} \quad d \leqslant 0 \end{cases} \tag{C.26}$$

The minima of the free energy functional are at $d = -1$ and $d = 1$, corresponding to the stable and metastable phase respectively. In between, the free energy functional has a constant slope.

In conclusion, we have shown that the RWRA model presented in this appendix captures most of the physics of the RWT model below the critical point.

ACKNOWLEDGMENTS

We would like to thank U. Bilstein, C. Godrèche, D. Mukamel and especially V. Rittenberg for helpful discussions and R. Behrend for reading the manuscript.

REFERENCES

1. M. R. Evans, D. P. Foster, C. Godrèche, and D. Mukamel, *Phys. Rev. Lett.* **74**:208 (1995); and *J. Stat. Phys.* **80**:69.
2. B. Derrida, E. Domany, and D. Mukamel, *J. Stat. Phys.* **69**:667 (1992).
3. G. Schütz and E. Domany, *J. Stat. Phys.* **72**:277 (1993).
4. B. Derrida, M. R. Evans, V. Hakim, and V. Pasquier, *J. Phys. A: Math. Gen.* **26**:1493 (1993).
5. P. F. Arndt, T. Heinzel, and V. Rittenberg, *J. Phys. A: Math. Gen.* **31**:L45 (1998).
6. C. Godrèche, J. M. Luck, M. R. Evans, D. Mukamel, S. Sandow, and S. R. Speer, *J. Phys. A: Math. Gen.* **28**:6039 (1995).
7. C. H. Bennett and G. Grinstein, *Phys. Rev. Lett.* **55**:657 (1985).
8. P. F. Arndt, T. Heinzel, and V. Rittenberg, *J. Stat. Phys.* **90**:783 (1998).
9. S. A. Janowsky and J. L. Lebowitz, *Phys. Rev. A* **45**:618 (1992).
10. G. Schütz, *J. Stat. Phys.* **71**:471 (1993).
11. K. Mallick, *J. Phys. A: Math. Gen.* **29**:5375 (1996).
12. V. Privman and L. S. Schulman, *J. Phys. A: Math. Gen.* **15**:L238 (1982); and *J. Stat. Phys.* **29**:205.
13. F. H. L. Eßler and V. Rittenberg, *J. Phys. A: Math. Gen.* **29**:3375 (1996).
14. R. B. Griffiths, C.-Y. Weng, and J. S. Langer, *Phys. Rev.* **149**:301 (1966); J. D. Gunton, M. San Miguel, and P. S. Sahni, in *Phase Transitions and Critical Phenomena*, Vol. 8, p. 267, C. Domb and J. L. Lebowitz, eds. (Academic Press, 1989).
15. Y. Saad, *Numerical Methods for Large Eigenvalue Problems* (Manchester University Press, 1992).
16. R. Bulirsch and J. Stoer, *Numer. Math.* **6**:413 (1964); M. Henkel and G. Schütz, *J. Phys. A: Math. Gen.* **21**:2617 (1988).
17. M. den Nijs, in *Proceedings of the 4th Workshop on Statistical Physics* (Seoul, January 27–31, 1997).
18. M. N. Barber, Finite-size scaling, in *Phase Transitions and Critical Phenomena*, Vol. 8, C. Domb and J. L. Lebowitz, eds. (1983).
19. N. G. van Kampen, *Stochastic Processes in Physics and Chemistry* (1981); C. W. Gardiner, *Handbook of Stochastic Methods for Physics, Chemistry and the Natural Sciences* (1990).